

# We are IntechOpen, the world's leading publisher of Open Access books Built by scientists, for scientists

6,900

Open access books available

186,000

International authors and editors

200M

Downloads

Our authors are among the

154

Countries delivered to

TOP 1%

most cited scientists

12.2%

Contributors from top 500 universities



WEB OF SCIENCE™

Selection of our books indexed in the Book Citation Index  
in Web of Science™ Core Collection (BKCI)

Interested in publishing with us?  
Contact [book.department@intechopen.com](mailto:book.department@intechopen.com)

Numbers displayed above are based on latest data collected.  
For more information visit [www.intechopen.com](http://www.intechopen.com)



# Method for Measurement of Single-Injector Heat Transfer Characteristics and Its Application in Studying Gas-Gas Injector Combustion Chamber

Guo-biao Cai, Xiao-wei Wang and Tao Chen  
*School of Astronautics, Beijing University of Aeronautics and Astronautics  
P. R. China*

## 1. Introduction

In the development of a Liquid Propellant Rocket Engine (LPRE), injector is always the element which requires the longest development period. An injector always especially in the initial design phase needs hundreds and thousands of tests to get a choice. These numerous tests, in turn, require reliable and accurate measurement method to give the basic support. The strength, the life cycle, and the cooling system effectiveness are highly dependent on heat transfer into and out of the system (Tramecourt et al., 2005). Heat transfer characteristics, combined with combustion efficiency, and combustion instability, are the three key parameters needed to be investigated in developing a new injector in a combustion chamber. The heat transfer characteristics generally contain the temperature and heat flux on the hot-gas-wall in the combustion chamber. The combustion efficiency and combustion instability can be observed easily by measuring the chamber pressure. However, it is always very hard to measure the temperature and heat flux on hot-gas-wall of the chamber in the hot-tests due to the extreme environment in LPRE chambers (temperature  $> 3000\text{K}$ , pressure  $> 10\text{atm}$ ).

Additionally, considerable efforts have been dedicated to model combustion in combustion chambers to understand and predict the heat transfer to the chamber walls (Zurbach, 2006), whereas the validation of computational fluid dynamics (CFD) design tools requires reliable experimental data assessment. This acquires a comprehensive set of data in the same facility, including wall heat fluxes along with inflow measurements (Tucker et al., 2005). To obtain the exact wall heat flux data, a reliable measurement method, in turn, is also required.

Though a number of efforts had contributed to design new injectors and study on heat transfer of injectors, studies focusing on the measurement method are less well documented. In recent years, Pennsylvania State University, University of Florida and NASA MSFC etc. made many attempts on studying the heat transfer characteristics of some injectors in heat sink chambers (Conley et al., 2007; Jones et al., 2006; Marshall et al., 2005; Santoro & Pal, 2005; Vaidyanathan et al., 2007, 2010b). They applied coaxial thermocouple to measure two point temperatures at the same axial location and difference radial locations in a heat-sink copper combustion chamber, and then used the temperatures to calculate the local heat flux

through a simple radial heat conduction analytical calculation. Coy summarized and analyzed the inverse heat transfer methods, and described a method for resolving inverse heat conduction problems using approximating polynomials (Coy, 2010), in which two sensors are also needed in any axial measurement location. All of previous method tried to get the exact time-dependent data of heat flux and surface temperature based on analytical solutions. Though these measurement methods can get the exact real-time heat flux data if right calculation methods are used, they always need two measurement points at the any axial measurement location, which increases the failure probability twice at any axial measurement location, and the current most popular method always put one measurement point right on the inner wall, and the thermocouple plug must be chamber-side geometry contoured to match the internal radius of curvature of the chamber, otherwise it will influence the inner flowfield and could not get the right temperature data. A little influence on the inner flowfield may induce a large deviation of the temperature on the measurement point. The potential influence of the thermocouple plug on the inner flowfield always exists, because the separated plug was put on the inner wall. In summary, all of the previous methods tried to get the exact time-dependent data with sacrificing the success probability and the measurement systems are complicated. In addition, they solved the axisymmetric problems with 1-D assumptions or solved 3-D problem with 2-D assumption.

This study introduces a simple method to obtain the inner wall temperature and heat flux in a heat sink combustion chamber. This method uses numerical calculation method to get the ultimate time-dependent inner wall temperature and heat flux with numerical calculation method. It considers the inner wall heat transfer coefficient as unchanged, which suffers a little change in hot-test, but the change is always less than 5%. Only single temperature measurement point at one axial location is just needed. In current method the measurement points are not on the inner wall surface, thus the potential influence on the inner flowfield doesn't exist anymore and there is not any sealing problem which also may cause severe measurement error. A reliable 2-D axisymmetric numerical calculation was applied to get the ultimate data. The measurement method, the related data processing and error analysis are demonstrated in detail with a specific hot-testing example of a gaseous hydrogen/gaseous oxygen single-element heat sink combustion chamber using this method. This method can be a feasible alternate one to get the inner wall temperature and heat flux, and it was originally developed for single-element axisymmetric chamber, and also can be a reference for non-axisymmetric chambers and multi-element injector chambers.

Furthermore, this method was used to investigate the heat transfer characteristics of a shear-coaxial single-element gas-gas injector combustion chamber. The full flow stage combustion (FFSC) cycle engine is preferable because of its high performance and high reliability, for which gas-gas injector technology is a key technology for this kind of engine and has received extensive studies (Archambault et al., 2002a, 2002b; Davis & Compbell, 1997; Farhangi et al., 1999; Foust et al., 1996; Meyer et al., 1996; Schley et al., 1997; Tucker et al., 1997; Santoro et al 2005; Tucker, 2007a ,2008b; Lin et al., 2005; Cai et al., 2008; Wang et al, 2009a, 2010b, 2010c etc.). Also, gas-gas injectors have been widely used on other engines and combustion devices (Calhoon, 1973; Groot, 1997). In this sense, it is of great value to investigate the heat transfer characteristics of a gas-gas injector combustion chamber. A single-injector heat-sink chamber was designed and hot-fire tested for 17 times at chamber pressure from 0.92MPa to 6.1MPa. Inner hot-gas-wall temperature and heat flux along with the axial direction of the chamber were obtained. The heat flux results were compared with each other qualitatively and quantitatively. The inner combustion flows were also numerically

simulated with multi-species turbulence N-S equations at higher chamber pressure from 5MPa to 20MPa to extend the experimental results. Both the combustion flow structures and heat flux profiles on inner wall were obtained and discussed.

## 2. Measurement method

The heat-sink chamber is preferable (Calhoon, 1973; Marshall et al., 2005; Santoro et al 2005; Conley et al., 2007; Jones et al., 2006) in the initial design phase of a new injector or in the study on the heat transfer characteristics of injector owing to its simple structure, low cost and easy manufacture. Thus, heat-sink combustion chamber was selected in this study. And the temperature measurement scheme is shown in Fig. 1.

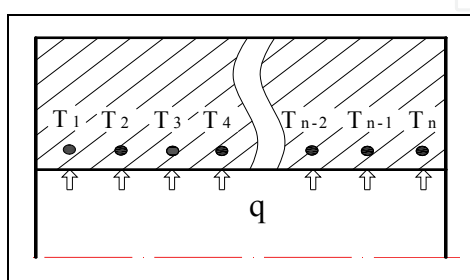


Fig. 1. Temperature measurement scheme in the heat sink chamber

This method applies thermocouples to measure the temperatures of a series of points near the inner wall along the axial direction in the heat-sink chamber. The distances between these points and inner wall surface are the same. The basic theory of this method is stated this way: with the development of combustion flow in the chamber, different heat fluxes are produced on the inner wall axially, further resulting in different temperatures on these measurement points. Therefore, the temperatures of these points can be utilized to obtain the heat flux and temperature on the inner wall.

In view that a heat-sink chamber can not undertake a long hot test, the tests are always completed within several seconds in which, fortunately, enough effective temperature output curves can be produced. In light of the temperatures are measured at those points near the inner surface of the chamber, the temperature profile along measurement point can clearly reflect the inner surface heat flux profile. The longitudinal heat transfer effect will be considered in the heat flux calculation.

This measurement method was employed in a single-element gaseous hydrogen/gaseous oxygen shear-coaxial injector test. The chamber shown in Fig. 2 was a modular heat sink design assembled with two OFHC (oxygen-free high conductivity) copper cylindrical barrel spool sections and an ablation resistance material nozzle. The inner diameter was 26 mm and the cylinder part was 255 mm in length.

Many small holes were designed at the axial locations of the measurement points, with temperatures of those at the bottom measured by the thermocouples. Axial locations for instrumentation are indicated in Fig. 2. The distances between all the measurement points and the chamber inner wall were the same except the distance between the first point and the inner wall. Multiple instrumentations (4 each) were presented at some axial locations, and four thermocouples were separated at  $90^\circ$  to examine the non-axisymmetry which may probably happen due to presumable manufacture and installation errors. Four thermocouples were also fixed in the injector surface to observe the plate surface's heat load.

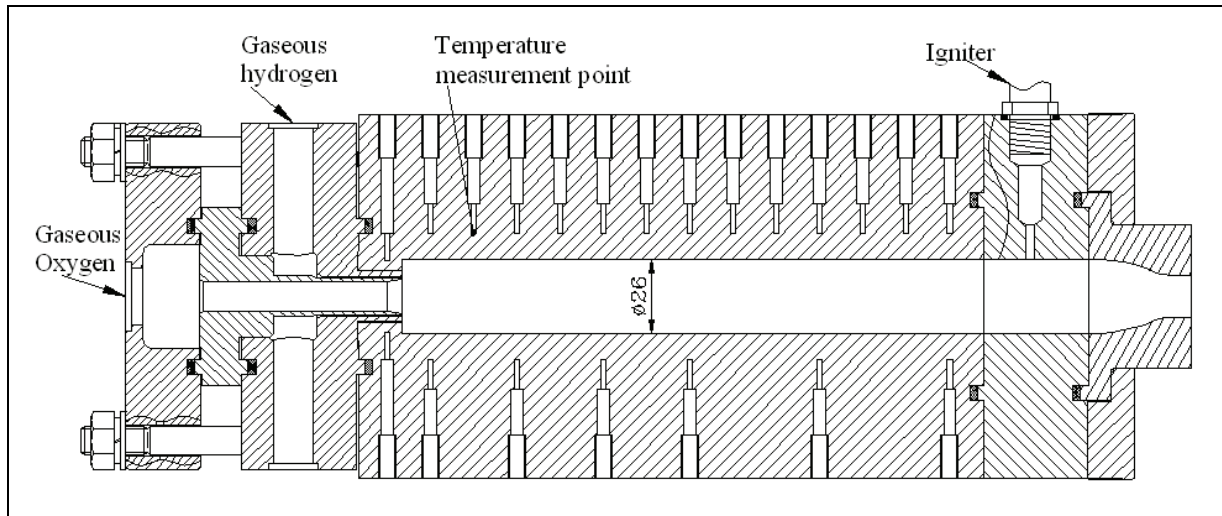


Fig. 2. Schematic of the chamber and thermocouple locations

The timing of the tests was designed as follows: the igniter preceded the injector, and with the chamber pressure got steady, the igniter was shut down. In the light of the fact that the igniter mass flowrate was less than 8.0g/s, the total ignition gas temperature was less than 1000K, and the ignition time lasted less than 0.8s, the influence of the ignition on wall temperature of the long cylinder part could be neglected here. A photo of the calorimeter chamber is shown in Fig. 3.

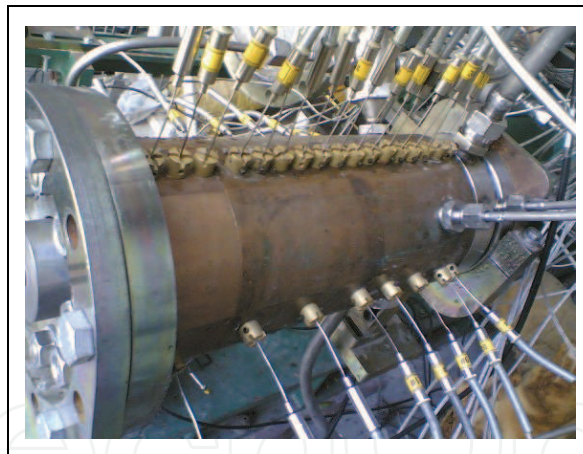


Fig. 3. The photo of the calorimeter chamber

### 3. Key design parameters and thermocouples

The test time was set to be 3s for this heat sink chamber. Some key parameters of the testing article, including the chamber wall thickness  $H$ , measurement hole diameter  $D$  and the distance  $L$  from the measurement point to the inner wall surface are listed in Table 1.

The Type-K thermocouples used in this hot-testing example were designed and provided by the Beijing West Zhonghang Technology Ltd. Their measurement ranges were all set to be 0-600°C. The temperature versus voltage response for the Type-K thermocouple is shown in Fig. 4, which shows a near-linear response. Their response time constants were designed less than 100ms and calibrated individually.

$H/\text{mm}$	48
$D/\text{mm}$	1.5
$L/\text{mm}$	8

Table 1. The values of key parameters

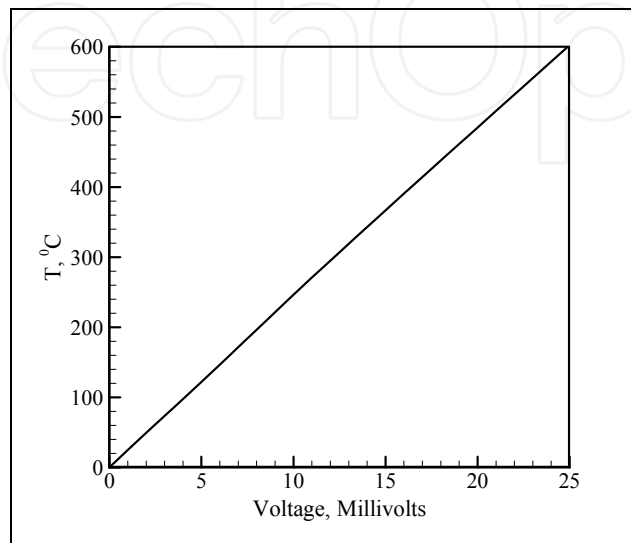


Fig. 4. Type-K thermocouple response

The chamber was fixed on a testing platform at the FFSC Laboratory in BUAA, resulting that the chamber was electronically grounded, which can produce strong interference signal in the output data. Therefore, an isolation module transmitter was designed for each thermocouple to eliminate the interference signal. The temperature responses of a thermocouple without and with isolation module are shown in Fig. 5.

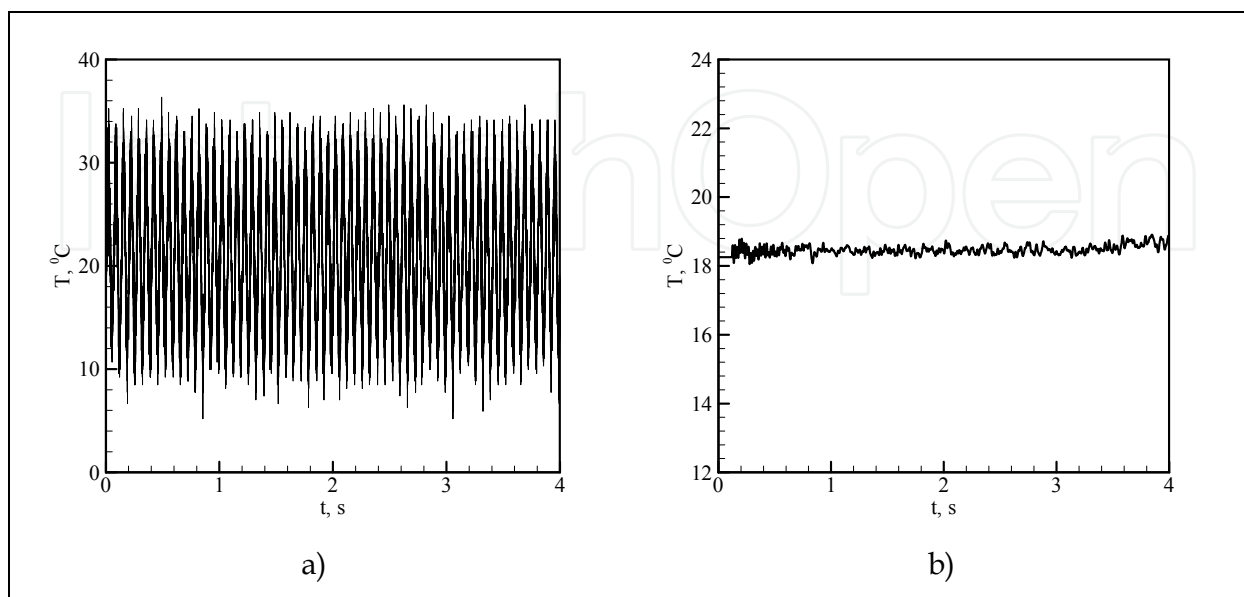


Fig. 5. Temperature outputs of transmitters a) without and b) with insulate module

#### 4. Calculation of inner wall temperature and heat flux

Several hot-fire tests were carried out for this gaseous hydrogen/gaseous oxygen single-element injector. A typical chamber pressure and one typical temperature curve are shown in Fig. 6. The temperature curve is depicted at the measurement point which is located 100mm away from the injector plane axially.

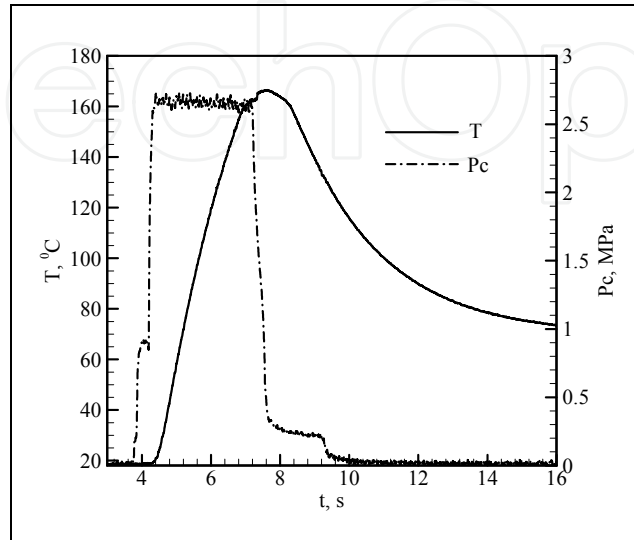


Fig. 6. Typical chamber pressure and wall temperature curve

Two steps are involved in converting these temperature output data into temperature and heat flux on the inner wall: 1. depicting the real measurement point temperature curves based on the output temperature curves, 2. obtaining the temperature and heat flux on the inner wall with 2-D axisymmetric heat transfer simulation. An error analysis will also be conducted in the end for this method.

##### 4.1 Temperature conversion

Any thermocouple has somewhat response delay, that is, when thermocouple of initial temperature  $T_0$  is used to measure an object of constant temperature ( $T_1$ ), the response curve function can write into equation (1):

$$\frac{T_1 - T}{T_1 - T_0} = \exp\left(-\frac{1}{\tau_c} \tau\right) \quad (1)$$

where  $\tau_c$  is thermocouple delay constant and  $\tau$  is time. The qualitative relationship between the object temperature and thermocouple output is shown in Fig. 7.

The heat transfer was unsteady in the test. The wall temperature kept rising after the combustion started. Obviously, there was some discrepancy between the real temperature curve and the experimental output curve for the existence of response delay, and it increased with the testing time, as shown in Fig. 8.

In this method, curve fitting and analytical calculation are employed to solve the real temperature curve from the thermocouple output. An example is shown in Fig. 9,  $T_1$  is a thermocouple output curve, and  $T_2$  is the biquadratic polynomial fitting curve of  $T_1$  (almost overlapped with  $T_1$ ).  $T_3$  is the real temperature result considering the response delay effect, which is higher than  $T_1$ . The thermocouple delay constant was set 100ms in this case.

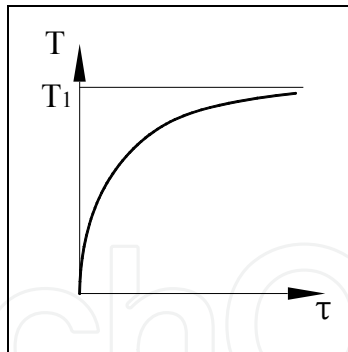


Fig. 7. The thermocouple characteristic curve schematic

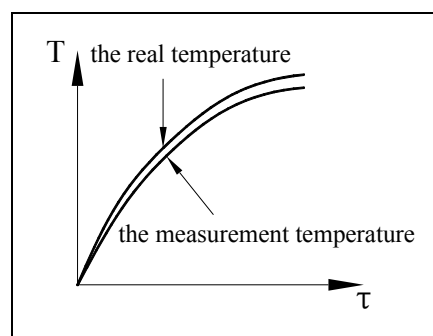


Fig. 8. Comparison of the TC measurement temperature curve and real wall temperature curve

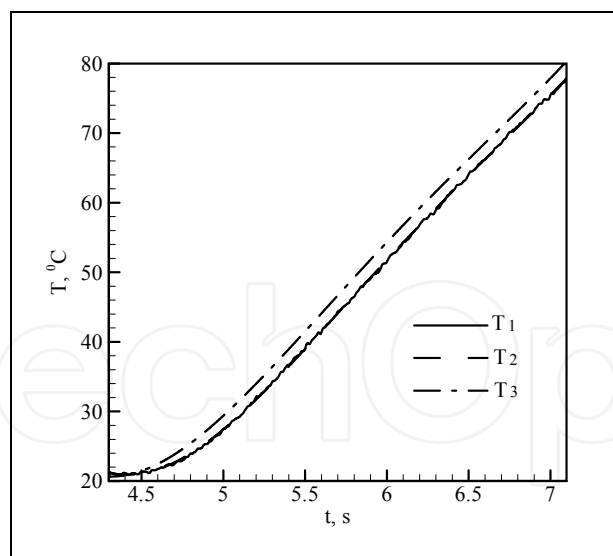


Fig. 9. Example of temperature curve conversion

#### 4.2 Inner wall heat flux and temperature calculation

The influence of the hot-testing start-up on the wall temperature was very limited, which can be observed from Fig. 10, thus, this influence was neglected here. When chamber pressure reached 90% of the stable value was considered as the beginning of the heat transfer and the calculation initial time, as  $t_0$  shown in Fig. 10. The end time of calculation

was chosen at the end of stable combustion, as  $t_1$  shown in Fig. 10. The heat transfer from  $t_0$  to  $t_1$  was calculated and the combustion was assumed to be stable in this period.

The inner wall heat flux can be defined with equation (2), in which the coefficient  $h$  can be defined by the Bartz equation as show in equation (3)(4).

$$q = h(T^* - T_w) \quad (2)$$

$$h = const. \frac{1}{d_t^{0.2}} \left( \frac{\eta^{0.2} c_p}{Pr^{0.6}} \right) \left( \frac{p_c^*}{c^*} \right)^{0.8} \left( \frac{A_t}{A} \right)^{0.9} \sigma \quad (3)$$

$$\sigma = \left[ \frac{1}{2} \frac{T_{wg}}{T^*} \left( 1 + \frac{\kappa - 1}{2} Ma^2 \right) + \frac{1}{2} \right]^{-0.68} \left( 1 + \frac{\kappa - 1}{2} Ma^2 \right)^{-0.12} \quad (4)$$

Here,  $T^*$  and  $T_w$  are inner flow total temperature and the inner wall temperature. From Equations (3)-(4), it can be seen that the coefficient  $h$  is almost unchanged when the chamber pressure  $p_c^*$  is constant. Figure 10 shows that the chamber pressure is steady and constant in the test, thus, the coefficient  $h$  is considered as unchanged in the hot-test, i.e. time-averaged heat transfer coefficient through the hot-test, which will be used as the boundary condition in the following heat conduction numerical modeling. In fact, in a real engine, the total combustion flow temperature, specific heat ratio and the  $Ma$  number are about 3600K, 1.2, and 0.1, the inner wall temperature changes from 300K to 600K, the heat transfer coefficient just changes less than 5% according to Equation (3)-(4).

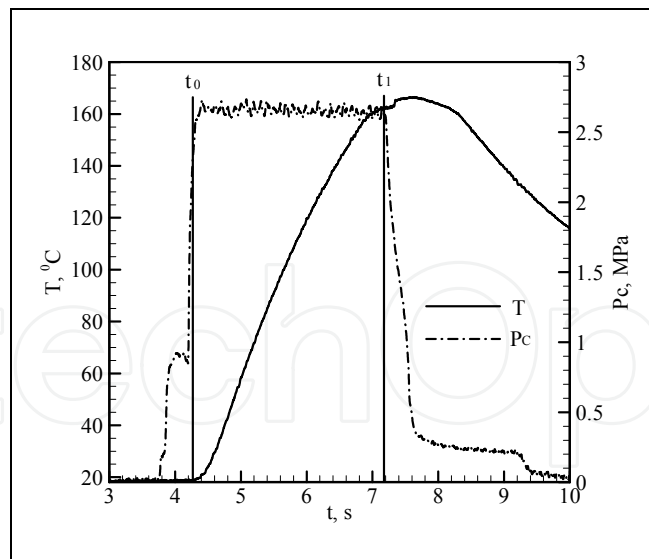


Fig. 10. The calculation time and temperature chosen from the output curve

The original thermocouple output data were obtained from the hot-fire test directly, and then the temperature  $T_m$  at the end time of calculation ( $t_1$ ) were gotten. Then the real temperatures  $T_r$  of each measurement point can be obtained through a conversion program described above.  $T_m$  and  $T_r$  are shown in Table 2. The injector plate was set at zero point axially.

Axial location/mm	$T_m/^\circ\text{C}$	$T_r/^\circ\text{C}$
-3	74.5	78.5
10	51.1	54.2
25	92.4	97.2
40	108.3	113.6
55	115.4	121.4
70	98.6	103.5
85	108.3	113.6
100	144.1	150.8
115	157.9	164.9
130	159.6	166.6
160	161.5	168.7
175	156.4	163.3
190	158.6	165.6
210	165.7	173
240	171.1	178.6

Table 2. The measurement and real temperatures

The calculation method for the inner wall temperature and heat flux from the real temperatures at measurement points are introduced below. The whole calculation procedure can be divided into two parts: 1-D and 2-D modelling. The real temperatures at the axial measurement points were labeled as  $T_{rk}$  ( $k=1, 2, \dots, n$ ) for the sake of convenience.

#### 4.2.1 1D axisymmetric modeling

Firstly, surface heat transfer coefficients at all measurement points were calculated with 1-D axisymmetric model regardless of the longitudinal heat transfer effect. These 1-D results will be used as the first iteration data for the 2-D calculation to accelerate the convergence. The unsteady axisymmetric 1-D heat conduction equation is as follows:

$$\rho c \frac{\partial T}{\partial t} = \frac{1}{r} \frac{\partial}{\partial r} \left( \lambda r \frac{\partial T}{\partial r} \right) + \dot{\Phi} \quad (5)$$

The total temperature of the inner combustion flow was chosen as the adiabatic combustion flame temperature  $T^*$ . Two empirical surface heat transfer coefficients  $h_{k1}$  and  $h_{k2}$  ( $h_{k1} < h_{k2}$ ) ( $k=1, 2, \dots, n$ ) were chosen firstly for each measurement point. Two temperatures  $T_{k1}$  and  $T_{k2}$  at time  $t_1$  shown in Fig. 10 were obtained from  $h_{k1}$  and  $h_{k2}$  with unsteady 1-D axisymmetric heat transfer model respectively. The 1-D mesh contains 60 grid points for the 48mm thickness chamber wall, and the stretching of the grid were used near the inner wall boundary. Each unsteady calculation period is from  $t_0$  to  $t_1$  shown in Fig. 10 (~2.95s in this case). Then the first iteration data  $h_k$  for 2-D modeling can be obtained using the linear interpolation with Equation (6). All the  $h_k$  ( $k=1, 2, \dots, n$ ) are shown in Table 3.

$$h_k = h_{k1} + \frac{T_k - T_{k1}}{T_{k2} - T_{k1}} (h_{k2} - h_{k1}) \quad (6)$$

#### 4.2.2 2D axisymmetric modeling

2-D axisymmetric unsteady modeling was applied to calculate the real inner wall temperature and the heat flux from  $t_0$  to  $t_1$ , as shown in Fig. 11.

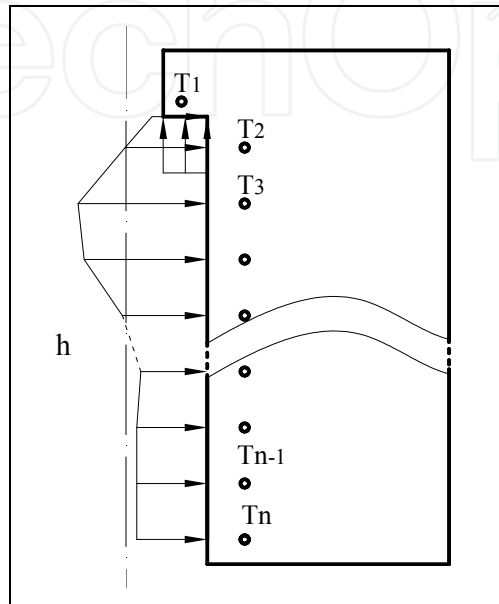


Fig. 11. Schematic of continuous calculation boundary condition of 2-D modeling

In this step, several 2-D unsteady simulations are needed to get a converged inner wall heat transfer coefficients. In each 2-D unsteady simulation, the inner wall of the chamber was treated as the third boundary condition, the calculation time is from  $t_0$  to  $t_1$ , and the initial temperature at time  $t_0$  of the whole chamber was set at ambient temperature. The 2-D mesh contains  $500 \times 60$  grid points, and the stretching of the grid was also used near the inner wall boundary. The unsteady axisymmetric heat conduction equation is as follows (Chapman 1987):

$$\rho c \frac{\partial T}{\partial t} = \frac{1}{r} \frac{\partial}{\partial r} \left( \lambda r \frac{\partial T}{\partial r} \right) + \frac{\partial}{\partial z} \left( \lambda \frac{\partial T}{\partial z} \right) + \dot{\Phi} \quad (7)$$

Source term  $\dot{\Phi}$  is set to  $h(T^* - T_w)$  on the inner surface, where  $h$  is heat transfer coefficient, a series of heat transfer coefficients  $h_k$  ( $k = 1, 2, \dots, n$ ) obtained from the 1-D modeling were used for the first 2-D simulation at the corresponding inner wall grid points.  $T_w$  is the inner wall temperature which keeps changing in each 2-D simulation process, ambient temperature  $T_{w0}$  for the initial condition of all the 2-D simulations. After the first unsteady 2-D simulation, a series of measurement point temperatures  $T_k'$  ( $k = 1, 2, \dots, n$ ) at the end of calculation time ( $t_1$ ) were obtained. Generally,  $T_k'$  ( $k = 1, 2, \dots, n$ ) differs from the real temperatures  $T_{rk}$  ( $k = 1, 2, \dots, n$ ). A correction of each heat transfer coefficients  $h_k'$  for the next unsteady 2-D simulation was made with Equation(8). And the unsteady 2-D simulation was repeated until the differences between the simulation results and the real temperatures  $T_{rk}$  ( $k = 1, 2, \dots, n$ ) reach the tolerance.

$$h_k' = h_k \cdot (T_{rk} - T_0) / (T_k' - T_0) \tag{8}$$

Axial location/mm	$h_{1D}/MW/(m^2K)$	$h_{2D}/MW/(m^2K)$
0	368	255
10	933	655
25	1701	1928
40	2038.5	2379
55	2175	2360
70	1838	1450
85	2019	1564
100	2831	3136
115	3028	3280
130	3062	2964
160	3100	3020
175	3000	2800
190	2840	2991
210	3180	2800
240	3296	3060

Table 3. Heat transfer coefficients on the hot-gas-wall

In addition, the temperature-dependent metal (OFHC copper) properties were also considered in the modeling. Table 3 lists the surface heat transfer coefficients at the corresponding axial locations from 1-D and 2-D calculations when the adiabatic flame temperature was considered as the total temperature. Because in the 2-D equation calculation, the inner wall heat flux is the source term and unique, if difference total temperature of the inner flow was set, the coefficients will be changed, but it did not influence the ultimate results of inner wall temperature and heat flux.

The inner wall temperature and the heat flux distributions at the end of calculation time are shown in Fig. 12, where X-coordinate denotes the distance from injector face plate. The results show that heat load on the injector face plate is very low. Temperature and heat flux distributions have similar profiles: They both begin to rise from the injector plate and reach the first peak at around 0.05m, and decrease until 0.075m, and then continue to climb successively to get the maximum values at 0.120m, followed by some small fluctuations and a little decrease in the end section. Though some small fluctuations exists for both the temperature and heat flux at the end, they mainly keep stable. It should be mentioned here that the fluctuations here were somewhat produced by using the same delay constant in the conversion calculation process, which were actually not involved in all thermocouples.

This heat load profile in the chamber was directly produced by the inner combustion flowfield structure. The first peak of the heat flux in the beginning is due to the existence of the strong recirculation zone there. Then the heat flux gets up continuously is because the

inner mixing and combustion become more and more intense and sufficient, and the flow becomes faster and faster downstream. When the combustion is mainly completed, the flowfield temperature and velocity reach their maxima. As the flow moves further downstream, the combustion heat release is generally finished, but the wall heat loss still exists, which induces the heat flux goes down a little in the end.

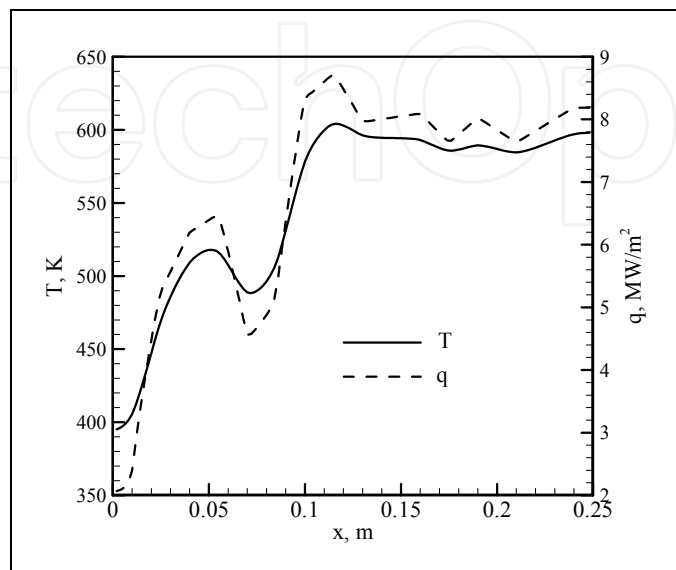


Fig. 12. The hot-gas wall temperature and heat flux distributions

### 4.3 Error analysis

Errors of this method mainly come from the temperature conversion process and the assumption of the 2-D axisymmetric calculation. Detailed analysis will be conducted in these two parts.

#### 4.3.1 Temperature conversion errors

Errors from the temperature conversion process occurred in the polynomial curve-fitting and application of the same response time constants for all thermocouples. For example as is shown in Fig. 9, the curve-fitting variance was  $90.0635\text{K}^2$  with 2800 temperature data points, indicating that this kind of error was very small and acceptable.

The deviation of response time also caused some errors to the results. Though the response time constants were provided by the manufacturer, analysis should be carried out to estimate its influence on the results.

Fig. 13 shows the different converted temperature curve results from one measurement output data with different response time constants of 100ms and 150ms respectively. Curve  $T_1$  is the original output of thermocouple.  $T_{100}$  is the converted curve for response time of 100ms and  $T_{150}$  for 150ms. It can be seen that though the difference of the time constants is even 50%, difference of the results is about 1.2 K, just 2% compared with the total temperature increment 60K.

#### 4.3.2 Calculation assumption error

2-D axisymmetric chamber physical model was employed in the heat conduction simulation, whereas real chamber body is three dimensional containing the measurement

holes. The 2-D axisymmetric assumption produced somewhat new error, for which, a 3-D calculation and a 2-D axisymmetric calculation for one chamber structure were carried out.

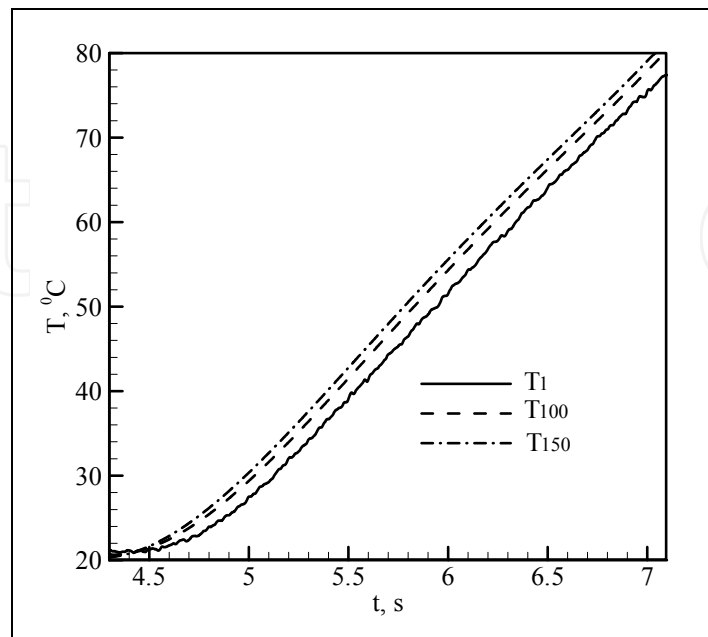


Fig. 13. Comparison of the converted temperature curves for different response times

Real chamber body 3-D physical model for calculations is shown in Fig. 14, where 1/4 of a chamber section with a measurement hole was selected. Uniform convection heat load was imposed on the inner wall surface. Bartz equation was used to get the convection heat coefficient  $h$ ,  $7500\text{W}/\text{m}^2\text{K}$  in this case. Initial temperature was set at  $300\text{K}$ . Another 2-D axisymmetric simulation was conducted with a whole chamber body without the measurement hole under the same boundary conditions. The results of these two cases after 3s unsteady calculations are shown in Table 4.

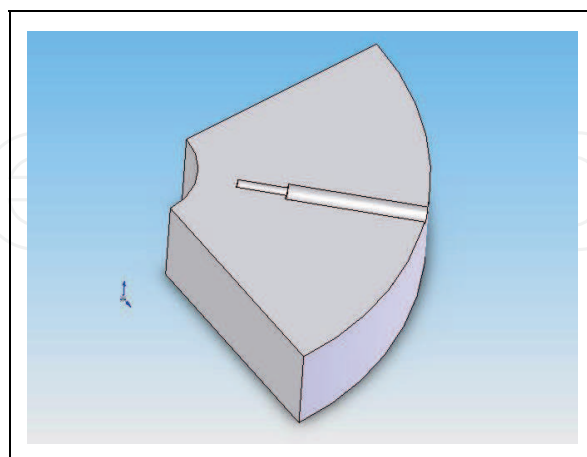


Fig. 14. The physical model of 3-D calculation

Table 4 indicates that the differences of temperature increment on the measurement hole bottom ( $\Delta T_h$ ), the heat flux ( $q_i$ ) and temperature increment ( $\Delta T_i$ ) at the corresponding inner wall surface were very low. The maximum error was just 3.6%. The reason is that the 3-D

character of this chamber body with this measurement method is not evident because measurement hole was rather small compared with the chamber body. The result indicates that for this measurement method, though the chamber structure is three dimensional, the 2-D axisymmetric calculation is feasible and the calculation cost can be sharply saved.

Parameters	Chamber with holes	Chamber without holes	Errors
$\Delta T_h/K$	361	348	3.6%
$q_i/MK/m^2$	17.1	17.5	2.3%
$\Delta T_i/K$	675	665	1.5%

Table 4. Comparison of some key results with 2-D and 3-D calculations

## 5. Application in studying gas-gas injector combustion chamber

This measurement method was used to investigate the heat transfer characteristics of a single-element gas-gas injector combustion chamber.

### 5.1 The testing article

The single-element shear-coaxial injector selected from the real engine shown in Fig. 15 was hot-tested here. The configuration of the single-element chamber can be seen in Fig. 2. All of the design parameters of this chamber were the nominal ones from the real engine. The combustor contract ratio was 3.1 and the character length was 800mm. The inner diameter was 26 mm and the cylinder part was 255 mm in length.

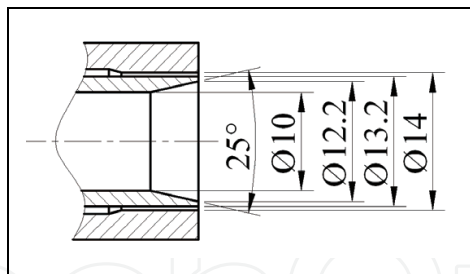


Fig. 15. Schematic of the injector

In the tests of different chamber pressures, with the heat-sink design of the chamber and the heat protection in consideration, the durations of the steady hot-fires were set from 1.5s to 5s for different chamber pressure cases: 0.92MPa–5s, 1.83MPa–4s, 2.69MPa–4s, 3.63MPa–3s, 4.52MPa–2s, 5.42MPa–2s, 6.1MPa–1.5s.

### 5.2 Test conditions

A total of 17 hot-fire tests were conducted steadily. The operation conditions and typical chamber pressure profiles are summarized in Table 5 and Fig. 16. The nominal Mixture Ratio (*MR*) of all conditions were 6.0, the uncertainties of the *MR* of tests were -2.8%-2.3%. The injection velocities and the propellant temperatures for all the cases were kept unchanged.

Chamber Pressure (MPa)	Ox Flowrate (g/s)	Ox. injection velocity/(m/s)	Fuel Flowrate (g/s)	Fuel injection velocity/(m/s)	MR	Repeat Times												
0.92	66.7	~70	11.2	~760	5.96	3												
1.83	135.1	~70	22.0	~760	6.14	2												
2.69	195.4	~70	32.8	~760	5.95	2												
3.63	258.3	~70	44.0	~760	5.87	3												
4.52	327.2	~70	54.4	~760 </tr <tr> <td>5.42</td> <td>397.8</td> <td>~70</td> <td>65.6</td> <td>~760</td> <td>6.06</td> <td>3</td> </tr> <tr> <td>6.1</td> <td>446.9</td> <td>~70</td> <td>76.6</td> <td>~760</td> <td>5.83</td> <td>2</td> </tr>	5.42	397.8	~70	65.6	~760	6.06	3	6.1	446.9	~70	76.6	~760	5.83	2
5.42	397.8	~70	65.6	~760	6.06	3												
6.1	446.9	~70	76.6	~760	5.83	2												

Table 5. Test conditions summary

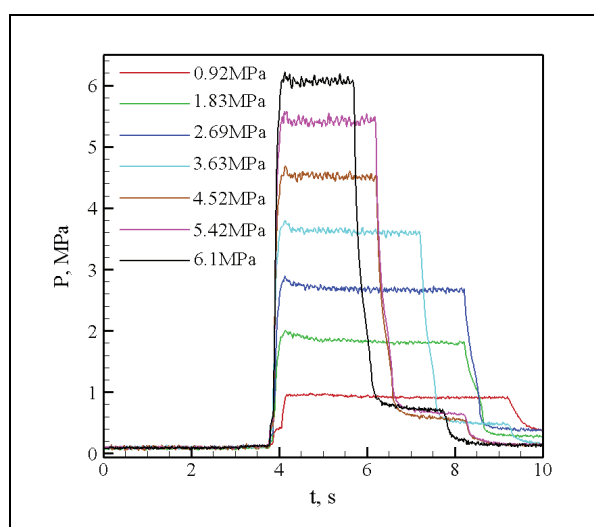


Fig. 16. The typical chamber pressure profiles of 7 cases

### 5.3 Results and discussion

The time traces of some thermocouples for a representative 2.69MPa chamber pressure test are shown in Fig. 17. A total of eight sets of thermocouple temperature measurements are shown. In terms of nomenclature in the figure, for example, the first trace labeled TC-10-00 denotes that the thermocouple was at the 10mm axial location, at 00 degrees (angle was defined with respect to major array of thermocouple). Except the curve TC-25-00, it can be seen that all temperature traces had the same response characteristic, were all well behaved and not noisy. The TC-25-00 had an obvious longer response time than others, so it could not be utilized.

During the steady state portion of the firing, the temperatures rose steadily owing to the heat sink nature of the chamber design. The curves of two thermocouples located respectively at 40mm and 100mm are nearly identical suggesting that the chamber flow was concentric. According to theory of heat transfer, higher heat flux on the inner wall at axial location of measurement point consequentially induces higher temperature raise at this point. Picture of the raises of temperatures at these measurement points versus the axial distance for 2.69MPa chamber pressure case is shown in Fig. 18, manifesting that the results of 2 repetitive tests were nearly identical.

All temperature curves were obtained for all the pressure cases, and then an axisymmetric heat conduction numerical calculation was conducted to obtain the hot-gas-wall heat flux for each pressure case. Inspection of empirical heat transfer correlations available in the literature such as the Bartz (Bartz, 1957), all the heat flux data were scaled by  $1/p^{0.8}$ , and the results are shown in Fig.19. It can be seen that all the heat flux distribution curves collapse to a single profile, and all the cases show the same qualitative distribution trends and the almost same quantitative local values, which means that the heat flux  $q$  of a gas-gas injector combustor correlates well with the pressure  $p$  as  $q \sim p^{0.8}$ . A valuable suggestion can thus be drawn that the heat flux data at high pressure condition can be predicted from that at a low pressure condition.

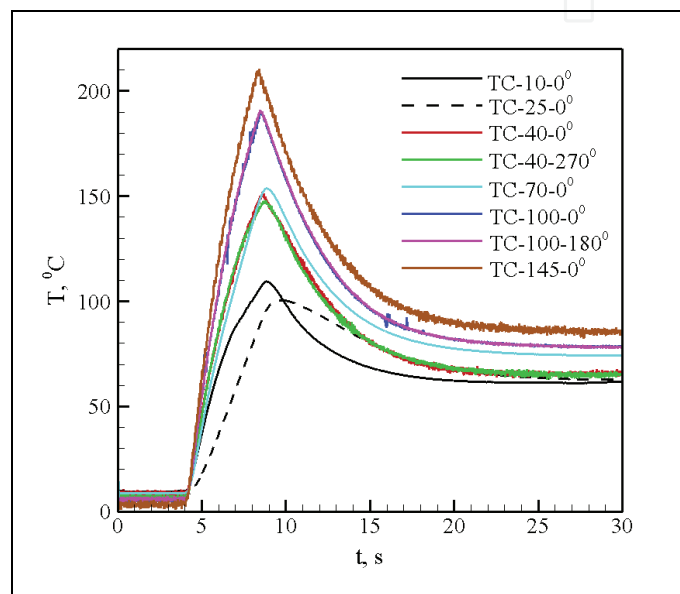


Fig. 17. Thermocouple temperature traces (representative) for a 2.69MPa test

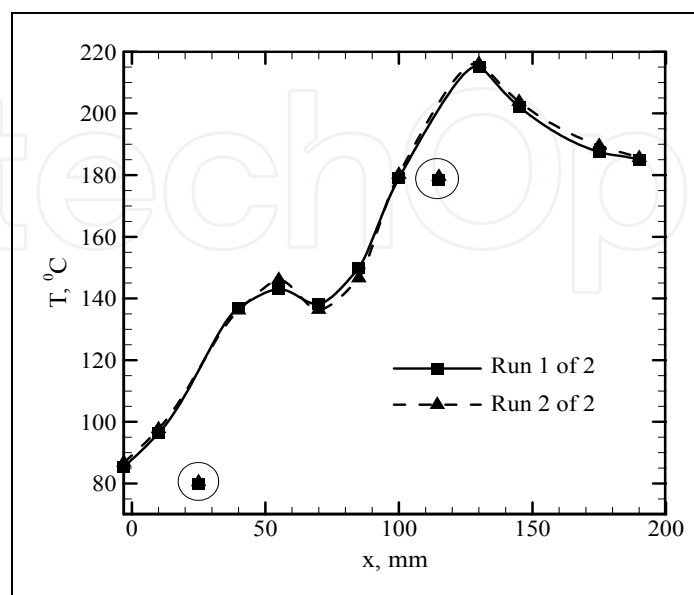


Fig. 18. Wall temperature versus axial distance for 2.69MPa chamber pressure

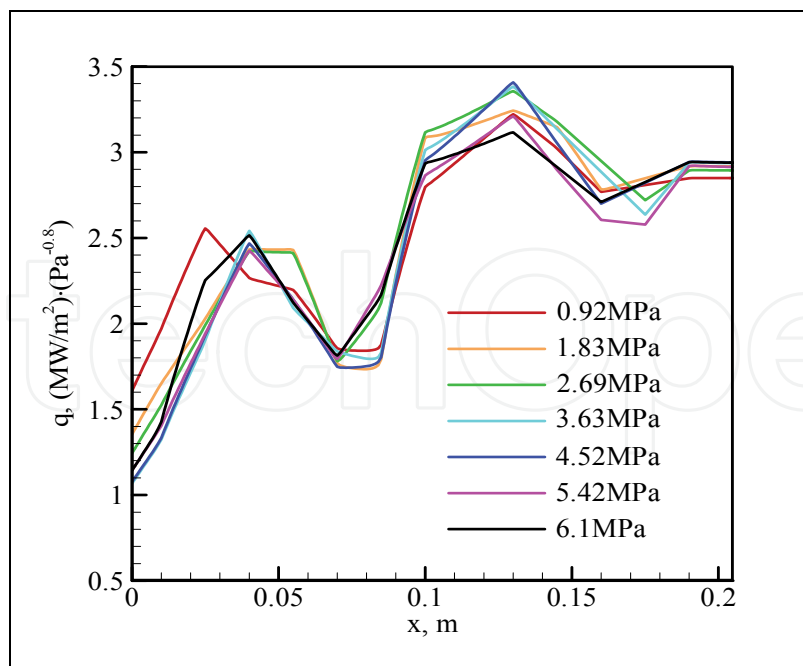


Fig. 19. Heat flux (scaled with respect to  $(1/Pc^{0.8})$ ) versus axial distance for each chamber pressure case

#### 5.4 Numerical study

In order to investigate the heat transfer characteristics at the high pressure condition unavailable in the experimental hot-test, and further examine the inner combustion flowfields at different chamber pressures, numerical simulations were conducted on this combustion chamber.

##### 5.4.1 Numerical models

A great effort has been made to perform the CFD simulation of gas-gas combustion flow at Pennsylvania State University, NASA Marshall Space Flight Center, University of Michigan and Beihang University et al. (Foust et al., 1996; Schley et al., 1997; Lin et al., 2005; Tucker et al., 2007a, 2008b; Cai et al., 2008; Sozer et al., 2009; Wang, 2009a, 2010b, 2010c) And the results indicated that the steady Reynolds Average Navier-Stokes (RANS) method combined with a  $k - \epsilon$  turbulence model could effectively simulate the whole combustion flow and obtain the statistical average solutions that can match the experimental results. In reference (Wang, 2010), difference RANS models were used to simulate a hot-testing chamber, and a feasible  $k - \epsilon$  turbulence model was obtained. Here, the RANS method combined with this  $k - \epsilon$  turbulence model was used.

Constant pressure specific heat of each species was calculated as a function of temperature

$$C / R = a_0 + a_1T + a_2T^2 + a_3T^3 + a_4T^4 + a_5T^5 \quad (9)$$

Coefficients of laminar viscosity and heat conduction of single component were calculated by molecular dynamics. The compressibility of the gas propellants at high pressure was considered. The R-K equation was substituted for the ideal state equation to take the real gas effect into account.

### 5.4.2 Numerical method and boundary condition

The entire system was solved by a strongly coupled implicit time-marching method with ADI factorization for the inversion of the implicit operator. Convective terms were 2-order flux split upwinding differenced, whereas diffusion terms were centrally differenced.

The calculation domain only occupied half the chamber. The radial and axial stretchings of the grid were used near the wall boundary and in the shear layer domain. The grid consisted of 29,028 cells, and the grid of half the cylinder was 43×350.

The inlets were fixed mass flowrate, and the inlet turbulence intensities both set to be 5%. The centerline was an axisymmetric boundary, and the nozzle exit was specified as a supersonic outlet. Non-slip wall boundaries were used on the chamber walls. The temperature of the combustor wall was set at environment temperature of 300K to achieve a steady heat flux.

### 5.5 Results and discussion

The dimensions of the chambers were kept unchanged, and a total of 4 numerical cases under different pressures from 5MPa to 20 MPa were chosen and shown in Table 6. The combustion flowfields and heat flux along with the combustor wall were obtained. The temperature contours are shown in Fig. 20, which shows that all the temperature contours of 4 pressure conditions are similar. And the similarity of the inner combustion flowfield structures leads to the same inner wall heat flux distribution shown in Fig. 21. From the time-mean inner flowfield results, the wall heat flux distribution can be clearly explained. The little peak of the heat flux in the beginning originates from the existence of the strong recirculation zone there. Then the heat flux gets up continuously with the increasing intensity and sufficiency of the inner mixing and combustion and the increasing velocity of the downstream flow. With the combustion mainly completed at the end of the combustor, the flowfield temperature and velocity both reach their maximum values. As the flow moves further downstream, the combustion heat release is generally finished, but the wall heat loss still exists, inducing a little downward movement of the heat flux in the end. In Fig. 21 all the heat flux data were scaled by  $p_c^{0.8}$ . It can be seen that all the curves almost collapse to a

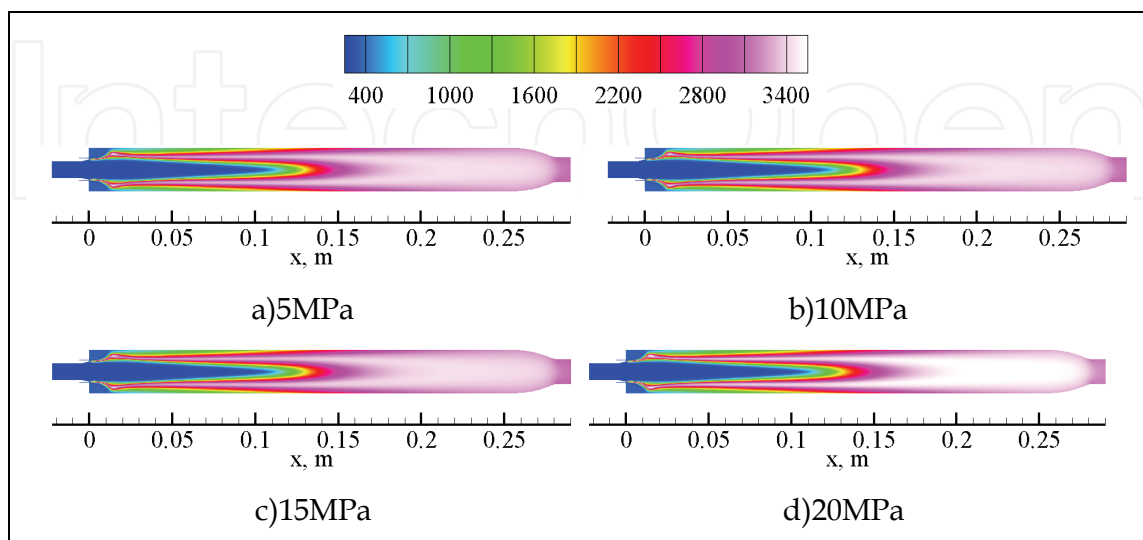


Fig. 20. Temperature contours of the five different pressure cases

single profile, which indicates that in the high pressure conditions, the heat flux in gas-gas injector combustors of different pressures also have the same qualitative distribution, and in a good agreement with  $q \sim p_c^{0.8}$  quantitatively.

Chamber pressure /MPa	H2 flowrate /(kg/s)	H2 temperature /K	H2 injection velocity /(m/s)	O2 flowrate /(kg/s)	O2 temperature /K	O2 Injection velocity /(m/s)
5	0.054	300	~760	0.324	300	~70
10	0.108	300	~760	0.648	300	~70
15	0.162	300	~760	0.972	300	~70
20	0.216	300	~760	1.296	300	~70

Table 6. Parameters of pressure scaling conditions

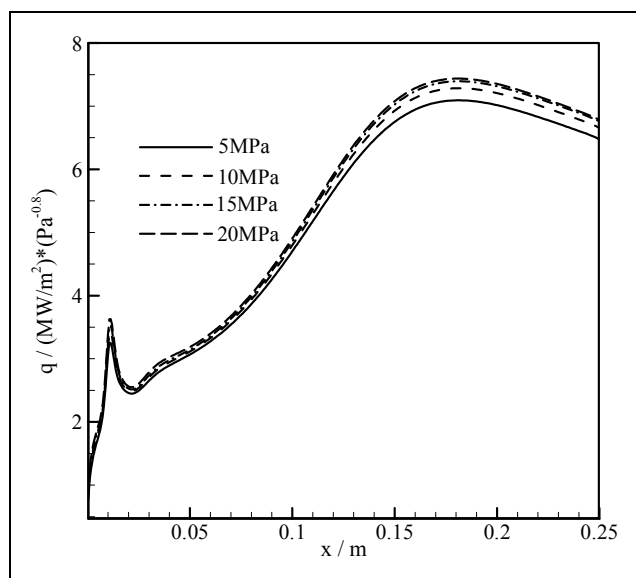


Fig. 21. Heat flux (scaled with respect to  $1/P_c^{0.8}$ ) versus axial distance for four chamber pressure cases

## 6. Conclusion

A method for measurement of single-injector heat transfer characteristics in a heat sink chamber was expound in this chapter. A series of measurement points are designed in the chamber with the same axial intervals and the same distance from the inner wall surface. This method measures the temperatures at these measurement points and then converts these temperatures into inner wall temperatures and heat flux with 2-D axisymmetric calculation. A hot-testing of a single-element gas-gas shear-coaxial injector chamber applying this method was introduced to explain this method. And the inner wall temperature and heat flux for this case were obtained and demonstrated. The basic principle and design, data processing and the corresponding error analysis were described in detail. And the error analysis showed that the accuracy of this method is sufficient for engineering

application, and the 2-D axisymmetric calculation can substitute for the expensive 3-D calculation with its cost-saving advantage. The method was originally developed for single-element axisymmetric chamber, and can also serve as a reference for non-axisymmetric chambers and multi-element injector chambers.

Furthermore, this method was used to investigate the heat transfer characteristics of a single-element shear-coaxial gas-gas injector combustion chamber. A single-injector heat-sink chamber was designed and hot-fire tested for 17 times at chamber pressure from 0.92MPa to 6.1MPa. Inner hot-gas-wall temperature and heat flux along with the axial direction of the chamber were obtained. The results show that heat flux in gas-gas injector combustors of different pressures not only have the same distribution qualitatively, also show a good agreement with  $q \sim p_c^{0.8}$  quantitatively. The inner combustion flows were also numerically simulated with multi-species turbulence N-S equations at higher chamber pressure from 5MPa to 20MPa to extend the experimental results. Both the flows structures and heat flux profiles on inner wall were obtained and discussed, and the results of numerical simulations indicated that the combustion flowfield of different pressures are similar and the heat flux is also proportional to pressure to the power 0.8.

## 7. Acknowledgments

The authors acknowledge the support of the state high-tech research and development fund. The authors also thank W. Zhang and Sh. Li from Beijing West Zhonghang Technology Ltd. for helps in designing the thermocouples. Finally, the authors thank all the people who made contribution and gave much help to this paper.

## 8. References

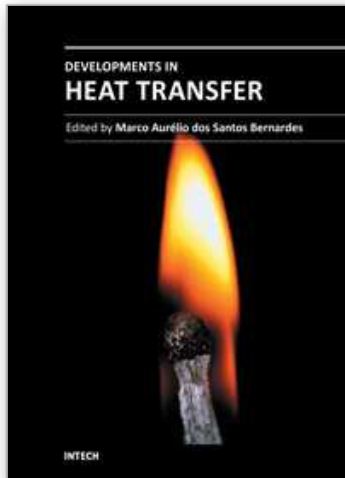
- Archambault, M. R., Perroomian, O., "Characterization of a Gas/Gas Hydrogen/Oxygen Engine," *AIAA Paper* 2002-3594, 2002a.
- Archambault, M. R., Talley, R. D., Perroomian, O., "Computational Analysis of a Single-Element Shear-Coaxial GH<sub>2</sub>/GO<sub>2</sub> Engine," *AIAA Paper* 2002-1088, 2002b.
- Bartz, D.R., "A Simple Equation for Rapid Estimation of Rocket Nozzle Convective Heat Transfer Coefficients," *Jet Propulsion*, Vol.27, No.1, Jan. 1957. pp: 49-51.
- Cai G B, Wang X W, Jin P, Gao Y S. Experimental and Numerical Investigation of Large Mass Flow Rate Gas-Gas Injectors. *AIAA Paper* 2008-4562.
- Calhoon, D., Ito, J., and Kors, D., "Investigation of Gaseous Propellant Combustion and Associated Injector-Chamber design Guide- lines," *NAS 3-13379*, Aerojet Liquid Rocket Company, Sacramento, California, 1973.
- Chapman A. J., *Fundamentals of Heat Transfer*, Macmillan, New York, 1987.
- Conley, A., Vaidyanathan, A., and Segal, C., "Heat Flux Measurements for a GO<sub>2</sub>/GH<sub>2</sub> Single-Element, Shear Injector," *Journal of Spacecraft and Rockets*, Vol. 44, No. 3, May-June 2007. pp. 633-639.
- Coy E., "Measurement of Transient Heat Flux and Surface Temperature Using Embedded Temperature Sensors", *Journal of Thermophysics and Heat Transfer*, Vol.24, No.1. January-February 2010. pp. 77-84.
- Davis, J. A., Campbell, R. L., "Advantages of A Full-flow Staged Combustion Cycle Engine System", *AIAA Paper* 1997-3318, 1997.

- Farhangi, S., Yu, T., Rojas, L., and Sprouse, K., "Gas-Gas Injector Technology for Full Flow Stage Combustion Cycle Application," *AIAA Paper* 1999-2757, 1999.
- Foust, M. J., Deshpande, M., Pal, S., Ni, T., Merkle, C. L., Santoro, R. J., "Experimental and Analytical Characterization of a Shear Coaxial Combusting GO<sub>2</sub>/GH<sub>2</sub> Flow field," *AIAA Paper* 1996-0646, 1996.
- Groot, W., A., McGuire, T., J., and Schneider, S., J., "Qualitative Flow Visualization of an 110N Hydrogen/Oxygen Laboratory Model Thruster", *AIAA Paper* 1997-2847, 1997.
- Jones G., Protz C., Bullard B., and Hulka J., "Local Heat Flux Measurements with Single Element Coaxial Injectors," *AIAA Paper* No. 2006-5194, July 2006.
- Lin, J., West, J. S., Williamst, R. W., and Tucker, P. K., "CFD Code Validation of Wall Heat Fluxes for a GO<sub>2</sub>/GH<sub>2</sub> Single Element Combustor," *AIAA Paper* 2005-4524, 2005.
- Marshall W. M., Pal S., and Santoro R. J., "Benchmark Wall Heat Flux Data for a GO<sub>2</sub>/GH<sub>2</sub> Single Element Combustor," *AIAA Paper* No. 2005-3572, July 2005.
- Meyer, L., Nichols, J., Jones, J. M., "Integrated Powerhead Demonstrator (booster hydrogen oxygen rocket engines)," *AIAA Paper* 1996-4264, 1996.
- NASA Space Vehicle Design Criteria. "Liquid rocket engine injectors," *NASA SP-8089*, 1976.
- Santoro R. J. and Pal S., "Validation Data for Full Flow Staged Combustion Injectors," *Final Report for NASA Contract Grant NAG8-1792*, Pennsylvania State University, 2005.
- Schley, C-A., Hagemann, G., Tucker, P. K., "Comparison of Calculation Codes for Modeling Hydrogen-Oxygen Injectors," *AIAA Paper* 1997-3302, 1997.
- Sozer E, Vaidyanathan A, Segal C, and Shyy W, Computational Assessment of Gaseous Reacting Flows in Single Element Injector, *AIAA Paper* 2009-449.
- Tramecourt, N., Masquelet, M., and Menon, S., "Large-Eddy Simulation of Unsteady Wall Heat Transfer in a High Pressure Combustion Chamber," *AIAA Paper* No. 2005-4124, July 2005.
- Tucker, K., West, J., Williams, R., Lin, J., Rocker, M., Canabal, F., Robles, B., and Garcia, R., "Using CFD as a Rocket Injector Design Tool: Recent Progress at Marshall Space Flight Center," *NASA NTRS 20050217148*, Jan. 2005.
- Tucker, P. K., Klemt, M. D., and Smith, T. D., "Design of Efficient GO<sub>2</sub>/GH<sub>2</sub> Injectors: a NASA, Industry and University Cooperative Effort," *AIAA Paper* 1997-3350, 1997.
- Tucker, P. K., Menon, S., Merkle, C. L., Oefelein, J. C., and Yang, V., "An Approach to Improved Credibility of CFD Simulations for Rocket Injector Design," *AIAA Paper* 2007-5572, 2007.
- Tucker, P. K., Menon, S., Merkle, C. L., Oefelein, J. C., and Yang, V., "Validation of High-Fidelity CFD Simulations for Rocket Injector Design," *AIAA Paper* 2008-5226, 2008.
- Vaidyanathan A., Gustavsson J., and Segal C., "Heat Fluxes/OH-PLIF Measurements in a GO<sub>2</sub>-GH<sub>2</sub> Single-Element Shear Injector," *AIAA Paper* No. 2007-5591, July 2007.
- Vaidyanathan A., Gustavsson J. and Segal C., "One- and Three-Dimensional Wall Heat Flux Calculations in a O<sub>2</sub>-H<sub>2</sub> System," *Journal of Propulsion and Power*, Vol. 26, No. 1, January-February 2010.
- Wang X W, Cai G B, Gao Y S. Large Flow Rate Shear-Coaxial Gas-Gas Injector. *AIAA Paper* 2009-5042.
- Wang X W, Cai G B, Jin P. Scaling of the flowfield in a combustion chamber with a gas-gas injector. *Chinese Physics B*, Vol. 19, No.1 (2010). SCI DOI: 10.1088/1674-1056/19/1/019401.

- Wang X W, Jin P, Cai G B . Method for investigation of combustion flowfield characteristics in single-element gas/gas injector chamber. *Journal of Beijing University of Aeronautics and Astronautics*, 35(9), (2009). pp.1095-1099
- Zurbach, S. (ed.), *Rocket Combustion Modeling, 3rd International Symposium*, Centre National D'Etudes Spatiales, Paris, March 2006.

IntechOpen

IntechOpen



## **Developments in Heat Transfer**

Edited by Dr. Marco Aurelio Dos Santos Bernardes

ISBN 978-953-307-569-3

Hard cover, 688 pages

**Publisher** InTech

**Published online** 15, September, 2011

**Published in print edition** September, 2011

This book comprises heat transfer fundamental concepts and modes (specifically conduction, convection and radiation), bioheat, entransy theory development, micro heat transfer, high temperature applications, turbulent shear flows, mass transfer, heat pipes, design optimization, medical therapies, fiber-optics, heat transfer in surfactant solutions, landmine detection, heat exchangers, radiant floor, packed bed thermal storage systems, inverse space marching method, heat transfer in short slot ducts, freezing and drying mechanisms, variable property effects in heat transfer, heat transfer in electronics and process industries, fission-track thermochronology, combustion, heat transfer in liquid metal flows, human comfort in underground mining, heat transfer on electrical discharge machining and mixing convection. The experimental and theoretical investigations, assessment and enhancement techniques illustrated here aspire to be useful for many researchers, scientists, engineers and graduate students.

### **How to reference**

In order to correctly reference this scholarly work, feel free to copy and paste the following:

Guo-biao Cai, Xiao-wei Wang and Tao Chen (2011). Method for Measurement of Single-Injector Heat Transfer Characteristics and Its Application in Studying Gas-Gas Injector Combustion Chamber, *Developments in Heat Transfer*, Dr. Marco Aurelio Dos Santos Bernardes (Ed.), ISBN: 978-953-307-569-3, InTech, Available from: <http://www.intechopen.com/books/developments-in-heat-transfer/method-for-measurement-of-single-injector-heat-transfer-characteristics-and-its-application-in-study>

**INTECH**  
open science | open minds

### **InTech Europe**

University Campus STeP Ri  
Slavka Krautzeka 83/A  
51000 Rijeka, Croatia  
Phone: +385 (51) 770 447  
Fax: +385 (51) 686 166  
[www.intechopen.com](http://www.intechopen.com)

### **InTech China**

Unit 405, Office Block, Hotel Equatorial Shanghai  
No.65, Yan An Road (West), Shanghai, 200040, China  
中国上海市延安西路65号上海国际贵都大饭店办公楼405单元  
Phone: +86-21-62489820  
Fax: +86-21-62489821

© 2011 The Author(s). Licensee IntechOpen. This chapter is distributed under the terms of the [Creative Commons Attribution-NonCommercial-ShareAlike-3.0 License](#), which permits use, distribution and reproduction for non-commercial purposes, provided the original is properly cited and derivative works building on this content are distributed under the same license.

IntechOpen

IntechOpen